

Simulations of Ion Current in Realistic Models of Ion Channels: The KcsA Potassium Channel

A. Burykin,¹ C. N. Schutz,¹ J. Villá,^{1,2} and A. Warshel^{1*}

¹Department of Chemistry, University of Southern California, Los Angeles, California

²Grup de Recerca en Informàtica Biomèdica, IMIM/UPF, Barcelona, Spain

ABSTRACT Realistic studies of ion current in biologic channels present a major challenge for computer simulation approaches. All-atom molecular dynamics simulations involve serious time limitations that prevent their use in direct evaluation of ion current in channels with significant barriers. The alternative use of Brownian dynamics (BD) simulations can provide the current for simplified macroscopic models. However, the time needed for accurate calculations of electrostatic energies can make BD simulations of ion current expensive. The present work develops an approach that overcomes some of the above challenges and allows one to simulate ion currents in models of biologic channels. Our method provides a fast and reliable estimate of the energetics of the system by combining semimacroscopic calculations of the self-energy of each ion and an implicit treatment of the interactions between the ions, as well as the interactions between the ions and the protein-ionizable groups. This treatment involves the use of the semimacroscopic version of the protein dipole Langevin dipole (PDLD/S) model in its linear response approximation (LRA) implementation, which reduces the uncertainties about the value of the protein “dielectric constant.” The resulting free energy surface is used to generate the forces for on-the-fly BD simulations of the corresponding ion currents. Our model is examined in a preliminary simulation of the ion current in the KcsA potassium channel. The complete free energy profile for a single ion transport reflects reasonable energetics and captures the effect of the protein-ionized groups. This calculated profile indicates that we are dealing with the channel in its closed state. Reducing the barrier at the gate region allows us to simulate the ion current in a reasonable computational time. Several limiting cases are examined, including those that reproduce the observed current, and the nature of the productive trajectories is considered. The ability to simulate the current in realistic models of ion channels should provide a powerful tool for studies of the biologic function of such systems, including the analysis of the effect of mutations, pH, and electric potentials. *Proteins* 2002;47:265–280.

© 2002 Wiley-Liss, Inc.

Key words: ion current; ion channel simulation; KcsA potassium channel; Brownian dynamics; protein electrostatics; dielectrics

1. INTRODUCTION

Movements of ions through specific transmembrane channels underlie many important biologic functions ranging from oxidative phosphorylation to electric signaling in neural and muscular systems.¹ Although a large amount of electrophysiological data provides a crucial information about the action of such channels (e.g., Hille,¹ Lauger,² Eisenman and Horn,³ and Latorre and Miller⁴), a detailed molecular picture of the control of ion permeating is still a partially unresolved problem.

Early modeling studies^{5–10} of the gramicidin channel (which was the only model system with clear structural information) led to some molecular insight. In particular, it was established that the energetics of the permeation process is the most important functional factor.^{8,11,12} It was also demonstrated that a microscopic evaluation of a reasonable penetration barrier can only be obtained with a careful treatment of the relevant electrostatic contributions.⁸

The recent elucidation of the crystal structure of the bacterial K⁺ channel (KcsA from *Streptomyces lividans*¹³) and other experimental studies (e.g., Heginbotham and Miller¹⁴ and Fedida and Hesketh¹⁵) have offered the exciting possibility of structure-based studies of biologically relevant channels. Here the ultimate challenge involves a detailed correlation of the structure of ion channels with the corresponding ion current. This includes understanding of the control of the current by external factors such as voltage, pH, concentration gradient, and drugs. It also includes the ability to predict and analyze the effects of various mutations.

Studies of several elements of the above problem have been reported recently. These include realistic microscopic calculations of the energetics of ion permeation in the KcsA channel^{16, 17} and more qualitative studies.^{18–21} As is

Grant sponsor: National Institutes of Health; Grant number: GM40283.

*Correspondence to: A. Warshel, Department of Chemistry, University of Southern California, Los Angeles, CA 90089-1062. E-mail: warshel@invitro.usc.edu

Received 16 October 2001; Accepted 15 January 2002

clear from these studies, the evaluation of the relevant energetics involves a major challenge, which requires the use of proper boundary conditions and proper long-range treatments. For example, the use of the local reaction field (LRF) treatment²² by Åqvist and Luzhkov^{16,17} appears to be one of the reasons these works provide more reasonable barriers than those obtained by other free energy calculations (e.g., Shrivastava and Sansom¹⁹ and Allen et al.²⁰).

Macroscopic models were also instrumental in providing insight about ion flow in models of ion channels.^{21,23–25} In particular, the instructive studies of Chung and coworkers²³ provided a useful insight about ion conductance in simplified macroscopic models of the potassium channel. This was done using Brownian dynamics (BD) simulations that treated the ions explicitly. The protein was represented by a set of fixed dipoles including helix macrodipoles embedded in a macroscopic model of the protein with a dielectric constant $\epsilon_p = 2$. However, the relationship between the resulting macroscopic energy and the actual electrostatic energy was not established. Note, for example, that the use of $\epsilon_p = 2$ leads to a major overestimation of the effects of so-called helix macrodipoles.²⁶ Similarly, the interaction between the K^+ ions inside the channel are likely to be overestimated with such a low value for the protein dielectric constant (see Section 3.3). Further, the effect of the protein-ionizable groups was not considered. At any rate, the models used have not been advanced to a stage that would allow them to capture the details of realistic channels and assess the effects of mutations or pH changes.

To progress in detailed modeling of ion conductance it is essential to overcome several major challenges. A realistic model should consider the effect of the ions' local environment, the interaction between ions and themselves, as well as the interaction between each ion and the protein-ionizable groups. Because all of these interactions should be evaluated during long simulation times (sometimes a microseconds time scale), it is impractical to use brute force molecular dynamics (MD) simulations for proper examination of ion current in the wide range of relevant conductance times. Free energy perturbation (FEP) calculations (e.g., Åqvist and Luzhkov¹⁶) can provide estimates of the activation barriers, but they cannot be used in direct simulations of ion flow. BD simulations can cover the relevant time range, but it is not clear how to construct free energy surfaces that will both reflect the actual molecular details of the given channel and be calculated in a sufficiently short computer time (to allow for effective simulations of long-time trajectories).

Our approach for overcoming the above challenges involves a realistic yet efficient evaluation of the free energy of the system and a BD simulation of the flow of the ions in this free energy landscape. Our free energy surface reflects a semimacroscopic estimate of the self-energy of each ion and a macroscopic expression for the interaction between the ions to themselves, as well as the interaction between the ions and the ionizable groups of the protein. This treatment, which is based on the idea introduced in our studies of proton translocations in proteins,^{27–29} allows us

to evaluate the energetics of the system on-the-fly and simulate ion current in KcsA.

Section 2 will describe our novel theoretical approach, emphasizing first the rationales for choosing the different strategies and then providing the detailed simulation procedures. Section 3 will describe our results, starting with the evaluation of the relevant free energy surfaces and then moving to the evaluation of the actual ion current. Section 4 will consider our results, compare our computational strategies to those used in related studies, and discuss the potential of our approach.

2. SIMULATION METHOD

The main idea of this work is the development of a fast yet reliable estimate of the energetics of ion channels and the use of the resulting energetics in a BD simulation of ion current. While the conceptual background of our approach is simple, the detailed procedures and considerations might look unnecessarily complicated to those who are only familiar with more “standard” simulation approaches. Thus, we will start by giving the overall background to our free energy calculations, while emphasizing the reason for choosing any specific strategies. We will then move to the description of the practical aspect of the simulations. Here we will try to clarify that our free energies surfaces are obtained by combining explicit all-atom simulations (which generate representative protein configurations) with semimacroscopic calculations of the corresponding electrostatic free energies. More specific details about the calculations can be found in our previous articles.

2.1. Evaluating Electrostatic Free Energies of Complex Ion Channel Systems

The reliability of simulations of ion penetration through channels depends primarily on the reliability of the corresponding electrostatic calculations. The selection of the most effective method depends strongly on the system being studied. Thus, for example, most current approaches would give reasonable results for surface groups in proteins but many will not perform well in protein interiors.³⁰ Similarly, different approaches might perform differently in studies of charge–charge interactions and studies of self-energies. Further, in our case we need to account for quantities that may be calculated only once (e.g., the electrostatic interaction between a single K^+ ion and the unionized protein) and for quantities, such as the interaction between the K^+ ions, that should be evaluated continuously during the simulations of the ion flow. These different energy terms can be handled in an effective way, we exploiting an idea introduced in our early studies of proton translocations^{27–29} and expressing the total electrostatic free energy of the ions in the system as

$$\Delta G(r) = \sum_i \Delta \Delta G_i(\mathbf{r}_i) + \sum_{i>j} \Delta G_{ij}(\mathbf{r}_{ij}) + \sum_{i,k} \Delta G'_{ik}(\mathbf{r}_i, \mathbf{R}_k), \quad (1)$$

where \mathbf{r} and \mathbf{R} represent, respectively, the coordinates of the ions and the ionizable residues of the protein. Here $\Delta \Delta G_i(\mathbf{r}_i)$ is the free energy invested in moving a single ion

from water to the specific position in the channel, \mathbf{r}_i . The notation $\Delta\Delta G$ is used because ΔG corresponds to the process of moving the ion from water to its channel site, and our calculations involve the displacement of a single water molecule by the ion (the ion penetration leads in most cases to a displacement of a water molecule). The overall $\Delta\Delta G_i$ term is expressed as

$$\Delta\Delta G_i(\mathbf{r}_i) = \Delta\Delta G_{\text{self}}(0,0,z_i) + \Delta\Delta G_{\text{steric}}(x_i,y_i,z_i). \quad (2)$$

The first term designates the change in self-energy upon moving the ion to the specific z_i on the channel axis ($x_i^2 + y_i^2 = 0$), where all other ionized groups of the protein are uncharged. The $\Delta\Delta G_{\text{steric}}$ term designates the change in free energy associated with the shift from the channel axis. Thus the overall $\Delta\Delta G_i$ corresponds to the penetration free energy profile for a single ion in an uncharged channel. Finally, $\Delta G'_{ij}$ represents the interaction between the ions and $\Delta G'_{ik}$ represents the interaction between the ions and the protein-ionizable groups.

As is clear from eq. 1 our first task is to find a reliable and efficient way of evaluating $\Delta\Delta G_{\text{self}}(\mathbf{r}_i)$. The selection of the optimal method for the calculations of $\Delta\Delta G_{\text{self}}$ is far from obvious. One may assume that the most reliable approach should involve the evaluation of the potential of mean force (PMF) by using umbrella sampling or related approaches (e.g., Roux and Karplus⁹ and Hu et al.³¹). It may be tempting to assume so because of the formal rigor of this approach and the fact that reliable evaluation of the average force associated with the motion of the ion should give the free energy at each point along its path. However, the reliability of molecular simulations depends on their convergence, which is different for different properties and procedures. At present the PMF approach is problematic when applied to transfer of charges from the bulk solvent to the channel interior or between different regions in the channel (see, e.g., the discontinuity in the calculated energy profile of ref. 9). Even a recent study of the PMF in KcsA³² has not provided the energy of the ion studied relative to its energy in water (see Section 4). In our opinion, the main problem with the PMF approach is associated with the fact that the calculations make one “blind” to such problems as incorrect treatments of long-range effects. This is so because the method does not tell us about the absolute solvation energy and the deviation from its expected value. Thus, one might use improper boundary conditions and not be aware of the resulting pitfalls. In view of this problem, it is probably preferable to perform FEP calculations (e.g., Warshel et al.³³) or linear response approximation (LRA) calculations^{34,35} for closely spaced positions of the ion along the channel relative to the corresponding calculation in the bulk water. Such an approach was first used for a few points in gramicidin by Åqvist and Warshel⁸ and more recently by Åqvist and Luzhkov¹³ in their study of the KcsA channel.

The use of FEP approaches for evaluating $\Delta\Delta G_{\text{self}}$ should be combined with a proper treatment of long-range effects and boundary conditions. Here, the use of our surface constraint all-atom solvent (SCAAS) model³⁶ and the LRF model²² are particularly effective. Finally, the

results obtained by such FEP studies can be interpolated by PMF calculations for the transfer of the ion across short distances to obtain the exact shape of the barrier, rather than its absolute height.

Unfortunately, despite the appeal of the FEP calculations they might still be problematic for highly charged systems and even for simpler calculations of internal charges (e.g., Sham et al.³⁵). The problems with fully microscopic FEP calculations are related to incomplete convergence in terms of solvent penetration and protein reorganization. Thus, it is sometimes advantageous to use semimacroscopic models. This is particularly true when one deals with interactions between central charge and many ionized groups. Semimacroscopic models scale down the electrostatic effects by a “dielectric constant” (see below) and give usually more stable results than all-atom models.

Here, we chose to use the semimacroscopic version of the protein dipoles Langevin dipole (PDLD/S) model in its LRA implementation (for more details see, e.g., Sham et al.³⁵ and Lee et al.³⁷). The PDLD/S-LRA self-energy is given by

$$\Delta\Delta G_{\text{self}}(\mathbf{r}_i) = \Delta G_{\text{el}}^{\text{ion}}(\mathbf{r}_i) - \Delta G_{\text{el}}^{\text{water}}(\mathbf{r}_i). \quad (3)$$

$\Delta G_{\text{el}}^{\text{ion}}$ and $\Delta G_{\text{el}}^{\text{water}}$ are, respectively, the electrostatic solvation free energies of the ion and of a water molecule (relative to the corresponding free energies in water). $\Delta G_{\text{el}}^{\text{ion}}$ is given by

$$\Delta G_{\text{el}}^{\text{ion}}(\mathbf{r}_i) = \frac{1}{2} [\langle U_{\text{el}}(q_i = \bar{q}_i; z_i) \rangle_{q_i = \bar{q}_i} + \langle U_{\text{el}}(q_i = \bar{q}_i; z_i) \rangle_{q_i = 0}], \quad (4)$$

where \bar{q} is the charge of the i th ion and $\langle \rangle_{q_i}$ designates an MD average over protein coordinates generated with the specific q_i ($q_i = \bar{q}_i$ or $q_i = 0$), which corresponds to the charged and uncharged states of the ion. $\Delta G_{\text{el}}^{\text{water}}$ is evaluated in an analogous way and thus will not be mentioned below. Note, that we have used z_i rather than \mathbf{r}_i for U_{el} to indicate that the value used corresponds to an average over the x_i and y_i coordinates during the LRA procedure, while constraining the ion to the given z_i . U_{el} is the PDLD/S effective electrostatic potential for the transfer of the ion from water to the given protein site. This potential is given by^{35,37}

$$U_{\text{el}} = - [\Delta G_{qw}^{w'} - (\Delta G_{qw}^p(q = \bar{q}) - \Delta G_{qw}^p(q = 0))] \left(\frac{1}{\epsilon_p} - \frac{1}{\epsilon_w} \right) + \Delta U_{q\mu}^p(q = \bar{q}) \frac{1}{\epsilon_p}, \quad (5)$$

where ΔG_{qw}^w is the self-energy of the given ion in water, ΔG_{qw}^p represents the change in the solvation energy of the protein with and without the ion, and $\Delta G_{q\mu}^p$ is the interaction between the protein residual charges and the ion. ϵ_w is the dielectric constant of water and ϵ_p is the protein dielectric “constant.” As explained elsewhere,^{30,35,38} the value of ϵ_p depends on the model used and when one uses the LRA approach (which is not implemented in current macroscopic models) it is possible to obtain reliable electro-

static energies with a low value of ϵ_p (e.g., $\epsilon_p = 4$). We would like to reemphasize here that the main advantage of the PDL/S-LRA over current Poisson–Boltzmann (PB) methods, such as the one used by Shrivastava and Sansom,¹⁹ is the fact that the protein reorganization is taken into account explicitly. This removes a large part of the uncertainty associated with the selection of ϵ_p .³⁰ Unfortunately, when one deals with electrostatic energies in protein environments the calculated results depend strongly on the assumed ϵ_p . Thus, it is important to move to an LRA treatment and obtain a somewhat more “unique” value for ϵ_p .

Because we deal with ions in a narrow channel, we follow the philosophy of Åqvist and Warshel⁸ and represented one water molecule on each side of the ion by an explicit all-atom model rather than by Langevin dipoles. This treatment will be further discussed in Section 2.3.

It is also useful to clarify here that ΔG_{self} reflects properly the corresponding free energy including the entropic effects associated with the protein motions. This is guaranteed by the use of the LRA approach, which reflects the reorganization free energy of the protein.

After evaluating the self-energy, we face the challenge of evaluating charge–charge interactions. A fully microscopic approach would be entirely impractical because we need to evaluate ΔG_{ij} for arbitrary positions of the ions. Further, even explicitly PDL/S calculations of charge–charge interaction are impractical for our purpose. The same is true for PB calculations, which cannot be used at present to provide a sufficiently fast evaluation of charge–charge interactions (see also Section 4). Fortunately, our studies, as well as the studies of other research groups (e.g., Schutz and Warshel,³⁰ Hassan et al.,³⁹ and Alden et al.⁴⁰), established the validity of the use of Coulomb’s law with a large effective dielectric constant for charge–charge interactions in proteins (e.g., Schutz and Warshel³⁰). Thus, we use

$$\Delta G_{ij} = 332 \bar{q}_i \bar{q}_j / (r_{ij} \epsilon_{\text{eff}}(r_{ij}))$$

$$\Delta G'_{ik} = 332 \bar{q}_i \bar{q}_k / (r_{ik} \epsilon_{\text{eff}}(r_{ik})), \quad (6)$$

where the free energies are given in kcal/mol and the r_{ij} s in Å. The \bar{q} s designate the indicated charges, i and j run over the K^+ and Cl^- ions, and k runs over the protein-ionizable groups (the \bar{q}_k s are 0 or -1 for acids and 0 or $+1$ for bases). The dielectric function is taken as⁴¹

$$\epsilon(r) = 1 + \epsilon'(1 - \exp(-ar)), \quad (7)$$

with $\epsilon' = 60$ and $a = 0.10 \text{ Å}^{-1}$.

The steric repulsion term in eq. 2, ΔG_{steric} , is evaluated as follows. A grid of 0.3-Å spacing is built and all points that are within 0.3 Å from the protein atoms are retained (all the other points are deleted). An additional grid with a 3.3-Å spacing is built around the protein atoms in the region $-20 \leq z \leq 15$ to represent the membrane region. The steric interaction between the K^+ ion and the grid points is then calculated using

$$G_{\text{steric}}(r_{ij}) = \sum_j \epsilon^*(r_{ij}^*/r_{ij})^8$$

$$\Delta G_{\text{steric}}(x_i, y_i, z_i) = G_{\text{steric}}(x_i, y_i, z_i) - G_{\text{steric}}(0, 0, z_i) \quad (8)$$

Taking ϵ^* as 1.0 kcal/mol we evaluate r^* using the actual all-atom model (see Section 2.3). This is done by constraining the z value of the ion to specific points in the selectivity filter and evaluating the PMF for moving in the x and y directions. The results of these PMF calculations are used to refine the optimal r^* . This procedure led us to select $r^* = 1.0$ Å for the interactions between the ion and the protein atoms for $\sqrt{x^2 + y^2} \leq 5$ Å. For further atoms we used $r^* = 2.8$ Å. The overall use of eq. 8 generates an “envelop” that gives a reasonable representation of the protein steric effect. A more systematic selection of r^* will be described in future studies. The grid-based evaluation of the steric repulsion term appears to have a significant advantage over the common direct pair list generation. The main advantage is due to the fact that the expensive calculation of distances is reduced to simple consideration of integer indexes in an array. This reduces drastically the time needed for evaluation of the ΔG_{steric} term.

Finally, we note that our ΔG_i only corresponds to the motion of the ion through the channel. For motions of the ion toward the membrane region or toward the outer boundaries of the simulation system, we used a simple steric potential of the form of eq. 8 with $r^* = 3.0$ Å.

2.2. Simulating Ion Current

Now with an efficient way of evaluating the free energy surface of the system, we can turn to the calculation of its time evolution. As stated in the introduction, it is impractical to use direct MD simulations as a general way for evaluating ion current in ion channels. However, BD or the related Langevin dynamics (LD) simulations can be used effectively with our semimacroscopic free energies. That is, the time evolution of our system can be evaluated by the Langevin equation.⁴²

$$m_i \ddot{\mathbf{r}}_{i\alpha} = -m_i \gamma_i \dot{\mathbf{r}}_{i\alpha} - \partial \Delta G / \partial \mathbf{r}_{i\alpha} + \mathbf{A}_{i\alpha}(t), \quad (9)$$

where i runs over the ions, α runs over the x , y , and z Cartesian coordinates of each ion, m_i is the mass of the i th ion, γ_i is the friction coefficient for the i th ion, and $\mathbf{A}_{i\alpha}$ is a random force, which is related to γ_i through the fluctuation-dissipation theorem.⁴³ The friction coefficient can be determined from the velocity autocorrelation by direct all-atom MD simulations of the all-atom system, using⁴²

$$\gamma = (3k_B T / m) \left(\int_0^\infty \langle \dot{\mathbf{r}}(0) \dot{\mathbf{r}}(t) \rangle dt \right)^{-1}. \quad (10)$$

This equation is particularly applicable to diffusion in the bulk or in the central cavity, where the ion is surrounded by several water molecules and its environment is similar to the corresponding environmental in the bulk solvent. However, the present study is not concerned with the evaluation or validation of the dynamic properties of the explicit all-atom system, and the friction coefficient is

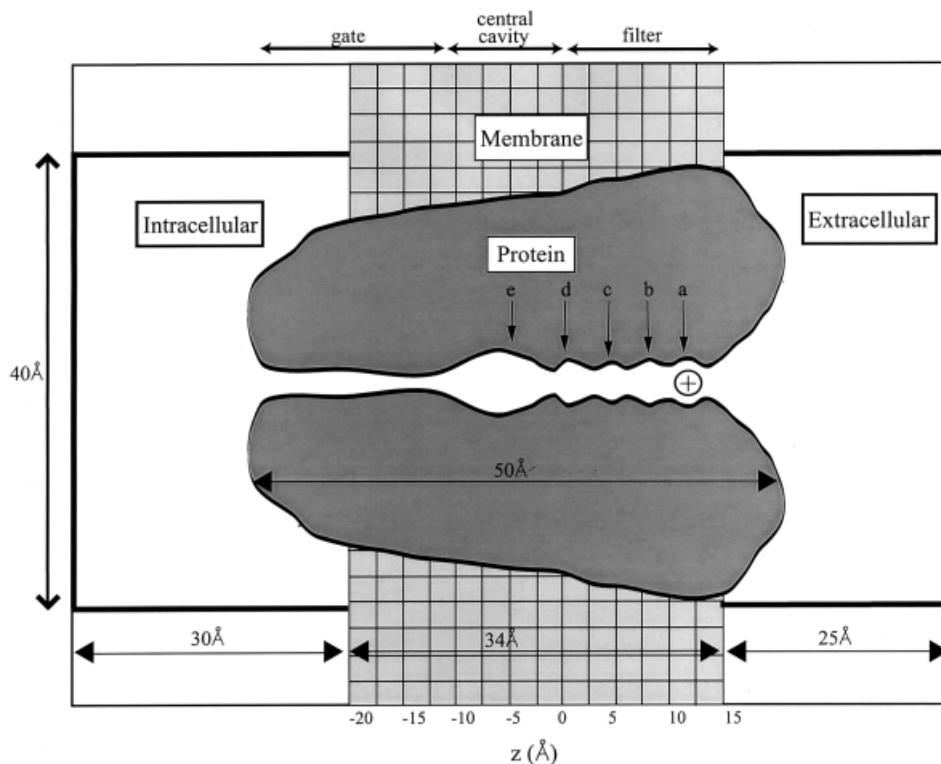


Fig. 1. Schematic description of the system studied. The wide black lines designate the actual boundaries of the simulation system.

only needed for the BD simulations. Thus, we used for the bulk system the corresponding experimental value¹ $\gamma = \gamma_w = 33 \text{ ps}^{-1}$ (here we denote the γ of the bulk and the channel regions by γ_w and γ_c , respectively). The estimate of γ for the channel interior is more challenging. Allen et al.²⁰ obtained for the selectivity filter a γ value that is about three times larger than the bulk value. Simulation in other regions of the channel led to γ values that are closer to the bulk value. However, it is not clear that the γ obtained from eq. 10 will provide the best parameter for eq. 9. In particular, we expect a strong correlation between the optimal value of γ and the optimal r^* if we look for the best way of reproducing the average microscopic dynamics in the filter by eq. 9. Because we prefer to address this issue in subsequent studies, we decided to consider several simulations for several limiting values of γ (i.e., values between 66 to 10 ps^{-1}). Attempts to obtain a more unique estimate of γ_c will be reported in the future.

The integration of eq. 9 was performed using time steps of, 1 fs for simulations with $\gamma_c = \gamma_w < 10 \text{ ps}^{-1}$, 10 fs for simulations with $10 \text{ ps}^{-1} < \gamma_c = \gamma_w < 30 \text{ ps}^{-1}$, and 5 fs for $30 \text{ ps}^{-1} < \gamma_c < 70 \text{ ps}^{-1}$, respectively. The simulation conditions were set with a predetermined concentration for the K^+ and Cl^- ions in each side of the membrane. The current was evaluated from its fundamental definition as the amount of charge that passes through the channel, per unit time. This was expressed as

$$J = \Delta Q / \Delta t \quad (11)$$

where ΔQ is the charge that passes the channel during the simulation period, Δt .

The present work is limited to simulations of ion flow under conditions that maintain a constant concentration gradient. To satisfy this requirement we used a stochastic boundary condition,⁴⁴ that is, when an ion passes the channel from left to right we transferred an ion of the same type from the far right of the system and inserted such an ion in the far left of the system. The same procedure was applied to a transfer in the opposite direction.

2.3. Practical Aspects of the Simulations

As is clear from the discussion above, we are dealing with two levels of simulations. The BD simulations involved a simplified model of the channel, where the specific interaction potentials are replaced by the corresponding effective free energies (the ΔG of eq. 1). The system used for this type of simulation is shown schematically in Figure 1 (for the case of a single ion). It includes the bulk solvent and the representation of the protein and the membrane, via the ΔG function. This reflects the interaction of the ion with the effective electrostatic potential of the protein and the membrane (represented by $\Delta\Delta G_{\text{self}}$) and the steric interaction with the protein and the membrane (represented by $\Delta\Delta G_{\text{steric}}$). The model also includes the interaction of the ion with the ionized groups of the protein (represented by ΔG_{ij}) as well as the interaction with other ions (represented by $\Delta G'_{ik}$).

To obtain the effective potential for the BD simulations, we need to perform explicit PDL/S-LRA calculations. For this purpose we had to combine two levels of calculations. That is, first we had to perform explicit all-atom calculations with the SCAAS and LRF model (to generate the

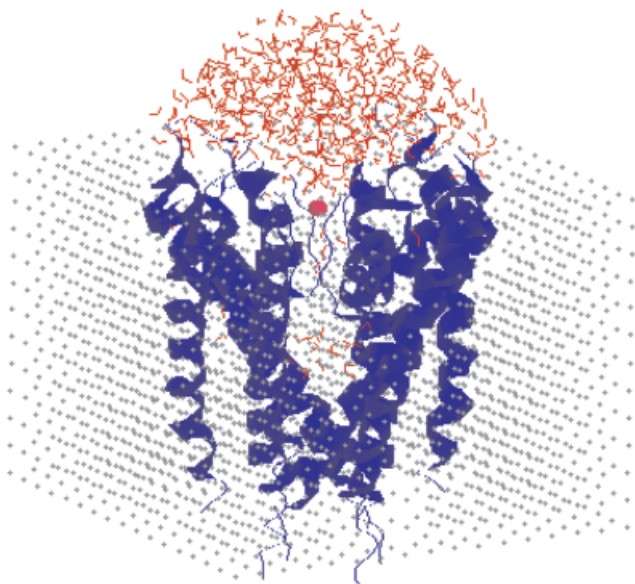


Fig. 2. System considered in the all-atom simulations. This system includes the specific ion and its surrounding protein + water + membrane regions. The simulations are done with the SCAAS spherical boundary conditions.

protein configurations needed for the LRA treatment) and then we perform the PDL/D/S calculations. These two sets of calculations involved two different simulation systems and different boundary conditions. The system used in the all-atom simulations is described in Figure 2. The explicit part of this system included the ion, the protein atoms, the membrane, and the water molecules within 24 Å from the specific position of the ion. The explicit water molecules were inserted in and around the protein and were subjected to the SCAAS boundary conditions. The membrane was represented by a cubic grid of induced dipoles with a 3.3-Å spacing and a polarizability of 2.7 Å³, determined from the Clausius–Mossotti equation. This type of treatment, which has been used before in our studies (e.g., Åqvist and Warshel⁸ and Alden et al.⁴⁰), provides reliable results for the most important features of the membrane (i.e., its effect as a low dielectric region). Long-range effects were treated by the LRF approach. The all-atom simulations were used to generate 30 configurations for the charged and uncharged state. Each of these simulations was run for 4 ps at 300 K, starting from the previous configurations.

The PDL/D/S-LRA averaging of the configurations generated by the all-atom simulations was done with the system presented schematically in Figure 3. This PDL/D/S simulation system involved a spherical system of a radius of 24 Å around the specific position of the ion. The detail constructions of such simulation systems are described extensively elsewhere (e.g., Lee et al.³⁷). The protein was treated with $\epsilon_p = 4$ and the contribution of the membrane region was evaluated by treating this region as a part of the protein with a dielectric constant $\epsilon_m = \epsilon_p = 4$. The use of a membrane dielectric of 4 (rather than 2) reflected the possibility that the membrane/protein interface contains

water molecules (see Alden et al.⁴⁰). The possible effect of changing the membrane dielectric to 2 can be estimated in specific cases by considering the energetics of the induced dipoles on the membrane (using the iterative approach of Warshel and Levitt⁴⁵) and evaluating the microscopic effect of changing ϵ_m from 4 to 2. The PDL/D/S sphere was surrounded by a continuum with $\epsilon = \epsilon_w$. The PDL/D/S calculations were averaged over the above-mentioned configurations of the charged and uncharged states as required by the LRA procedure of eq. 4.

All the self-energy calculations were done with the program MOLARIS, which combines the ENZYMIK and POLARIS programs.³⁷ The MD simulations (needed to generate the protein configurations) were performed by the ENZYMIK module with the parameter set of Lee et al.,³⁷ which included the effect of the induced dipoles. The van der Waals parameters for the all-atom simulations of the solvated K⁺ ion were optimized by fitting the calculated and observed solvation free energy of this ion in water. The refined parameters were $A = 920 \text{ kcal/mol}^{-1} \text{ Å}^6$ and $B = 8.0 \text{ kcal/mol}^{-1} \text{ Å}^3$ for the nonbonded interactions ($V(r_{ij}) = A_e A_f r_{ij}^{-12} - B_e B_f r_{ij}^{-6}$). The A and B for the water atoms were kept the same as before.³⁷

The all-atom simulations involved two set of calculations. One set (set A) used the induced dipoles without the corresponding induced dipole forces and the other set (set B) included the induced dipole forces. Set B tends to give larger interactions between the ion and the carbonyls of the selectivity filter. Both sets involved scaling down of the ENZYMIK residual charges by 0.8, which is our standard procedure in calculations that involve induced dipoles. Comparison of the energetics obtained by both methods provided a useful way of estimating the sensitivity of the PDL/D/S calculations to the protein configurations used.

The PDL/D/S-LRA calculations were performed on the configuration generated by all-atom trajectories of the charge and uncharged states, evaluating the corresponding PDL/D/S potentials (the U_{el} s of eq. 5), and calculating the average of eq. 4. As stated above each ion was flanked by two explicit water molecules in the PDL/D/S calculations. This treatment is particularly simple in our LRA protocol because the protein configurations used in the PDL/D/S calculations are generated with explicit water molecules. Thus, when we moved from the explicit all-atom simulations to the PDL/D/S calculations we kept two explicit water molecules as a part of the “protein” in the PDL/D/S calculations.

The simulations of the ion current in the effective model of the channel were performed by a special program (called CHANNELIX) that took as input the $\Delta\Delta G_{\text{self}}$ of the PDL/D/S-LRA calculations and evaluated on-the-fly the ΔG_{ij} , ΔG_{ik} , and ΔG_{steric} terms. More specifically, this program reads the coordinates of the protein and the membrane, as well as an interpolation table of the $\Delta\Delta G_i$ profile and the position of the ionized residues. Using this information, and with the procedure described above, allows the program to evaluate on-the-fly the terms of eq. 1 and the corresponding forces for any position of the

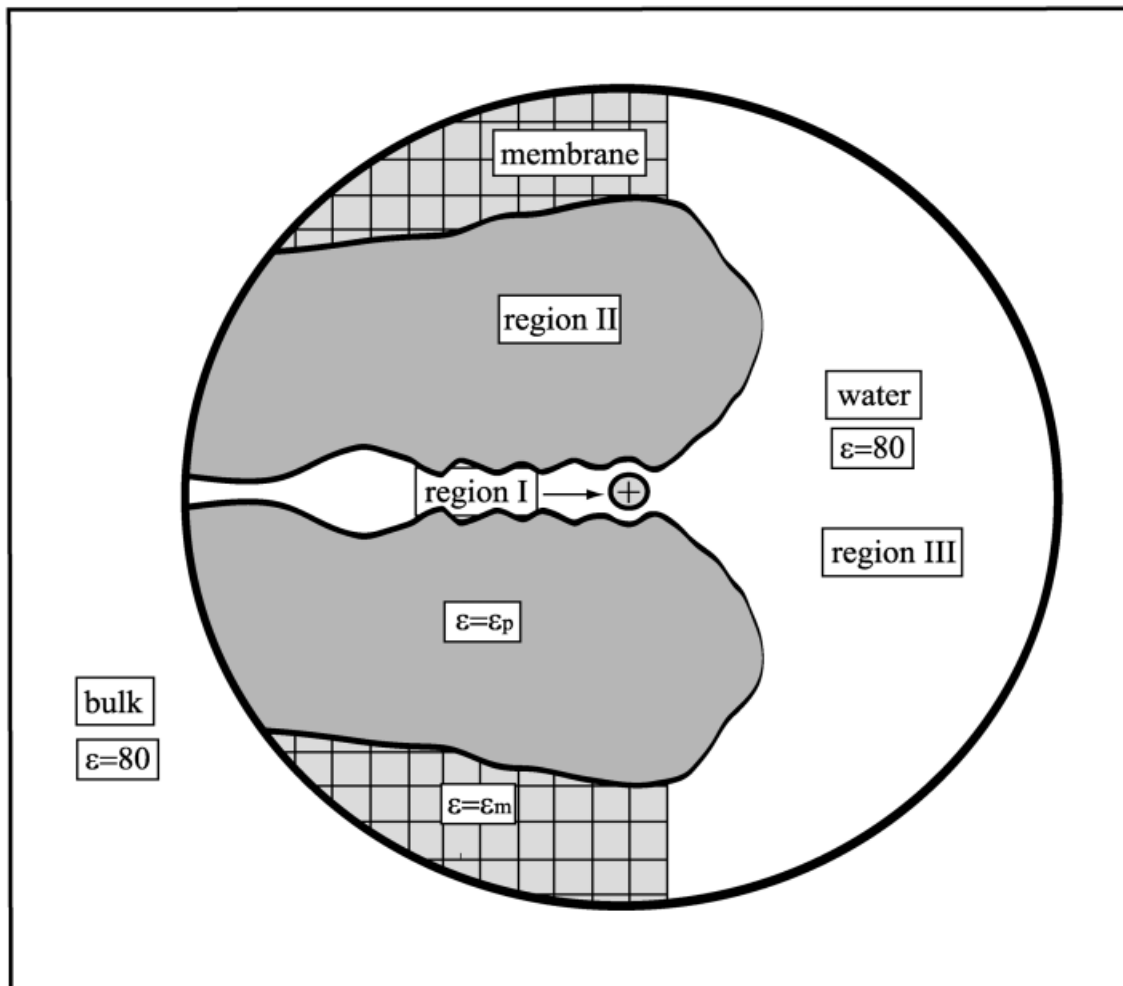


Fig. 3. PDL/D/S simulation system. The system includes the ion studied (region I), the surrounding protein + membrane (region II), the water region (region III) represented by Langevin dipoles, and the surrounding bulk.

simulated ions. These effective potentials and forces are then used in BD simulations of ion current.

Finally, we note that a single evaluation of the energy and forces for the channel and a 24-ion system takes for CHANNELIX $\approx 10^{-3}$ s on an R12000 processor of SGI origin 200 computer. This means that we can simulate in 24 hours run and a time step of 10 fs a trajectory of about 500 ns. Obviously, making the code fully parallel, improving the numerical integration procedure, and/or using stronger computers can yield faster performance.

3. RESULTS

3.1. Evaluating the Penetration Profile for a Single Ion

The first and perhaps most crucial step of our procedure is the evaluation of $\Delta\Delta G_{\text{self}}(\mathbf{r})$ for a single K^+ ion. The corresponding free energy profile, which reflects the interaction between the ion and the un-ionized channel, was evaluated by the PDL/D/S-LRA approach (see Section 2). These simulations involved a generation of protein configurations by full all-atom SCAAS+LRF simulations and a

PDL/D/S averaging of the electrostatic energies of these configurations (for each position of the ion). The configurations generated were used for the PDL/D/S-LRA calculations (see Section 2).

The PDL/D/S-LRA penetration profile for the K^+ ion was evaluated by the procedure outlined in Section 2.3. This was done for both sets A and B of the simulation procedure (i.e., generating protein configuration without and with induced dipole forces). In each case we repeated the simulations for 120 positions separated by 0.1 Å spacing in the filter region and a larger spacing for the gate and cavity regions. These positions were maintained in the all-atom MD simulations by constraining the ion to the positions $x = 0, y = 0, z = z'$, using an harmonic constraint with a $400\text{-kcal/mol}^{-1}\text{\AA}^{-2}$ force constant. The resulting penetration profiles for the two sets (Fig. 4) involves an interpolation between the ion positions.

The main point that emerges from the calculated profile is the reasonable values of the lowest and highest points. An alternative qualitative microscopic calculation produced potential barriers of more than 100 kcal/mol in the

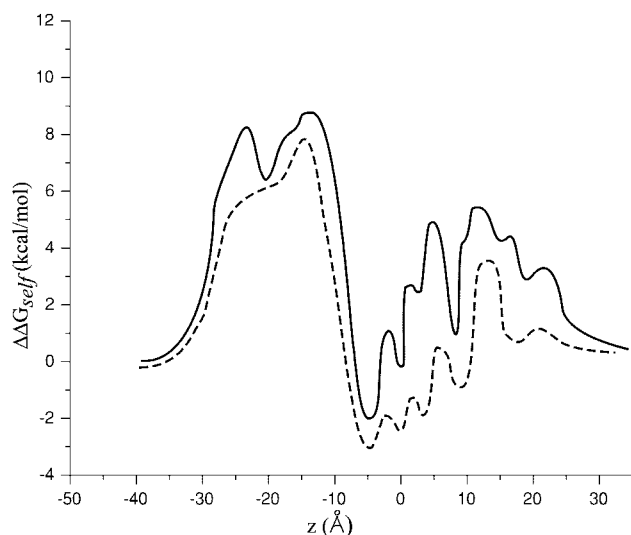


Fig. 4. PDL/S-LRA self-energy ($\Delta\Delta G_{\text{self}}$) profile. The results obtained with sets A and B are shown by solid and broken lines, respectively.

gate region¹⁹ and another simulation,²⁰ which considered a realistic description of the selectivity filter, obtained a trap of ≈ 30 kcal/mol at $z = 7.5$ Å (see Section 4).

Our results, for the passage of a single ion through the selectivity filter, cannot be compared directly to the results of Åqvist and Luzhkov¹⁶ because the calculations of these workers involved an additional ion in the central cavity. However, even with the addition of an ion in the central cavity (see Section 3.2) the PDL/S-LRA results give a lower barrier than that obtained in Åqvist and Luzhkov¹⁶ for the same situation. It might well be that the FEP calculations give a more reliable value for the single ion than the PDL/S-LRA calculations. However, in view of the possible problems associated with FEP calculations of highly charged states (see below) we prefer to use the $\Delta\Delta G_{\text{self}}$ obtained from the semimacroscopic calculations. At any rate, it would be trivial to use our approach with the ΔG_{self} s obtained by FEP calculations rather than with those obtained by the PDL/S results. This would require, of course, mapping of the entire length of the channel rather than only the selectivity filter.

The $\Delta\Delta G_{\text{self}}$ profile for the Cl^- ion was determined only in the selectivity filter and the gate regions. It was found that we have barriers of more than 15 kcal/mol in both regions. In view of this finding we used a simplified procedure and prevented the Cl^- ions from entering the channel by using a repulsive potential at the channel entries. A more advanced treatment, which allows for the possible penetration of Cl^- ions in the presence of K^+ ions, will be considered in future studies.

Finally, we note that our $\Delta\Delta G_{\text{self}}$ depends on the protein configurations obtained in the LRA procedure. The permanent dipoles of the configuration obtained from the simulations without induced-dipole forces (set A) are less polarized toward the ion charge than those obtained with induced-dipoles forces. As a consequence

TABLE I. Calculated $\text{p}K_a$'s of the Ionizable Groups of the KcsA Channel[†]

Residue ^a	Model 1		Model 2		Model 3	
	$\text{p}K_{\text{int}}$	$\text{p}K_{\text{app}}$	$\text{p}K_{\text{int}}$	$\text{p}K_{\text{app}}$	$\text{p}K_{\text{int}}$	$\text{p}K_{\text{app}}$
His25	4.2	0.7	4.0	0.2	3.0	0.3
Arg27	11.2	11.2	6.3	4.7	6.5	5.7
Glu51	3.7	0.7	4.5	1.7	2.1	0.2
Arg52	10.0	10.7	8.1	7.7	8.1	7.7
Arg64	9.0	8.7	10.4	11.2	10.5	11.2
Glu71	10.0	12.2	9.6	12.1	5.4	5.8
Asp80	6.4	5.2	5.9	4.7	4.4	1.8
Arg89	10.1	13.7	10.4	14.7	8.3	11.3
Arg117	10.8	10.7	9.7	9.2	9.6	9.0
Glu118	6.5	8.2	7.9	10.2	7.3	9.3

[†]The results are given for different models, where 1, 2, and 3 correspond to a model where the membrane region is replaced by water, a complete model (protein and membrane), and a complete model with two K^+ ions in the channel (in the 01001 configuration).

^aOnly the $\text{p}K_a$ s of the ionized residues in the first subunit are presented. The results for the residues in the other subunits are assumed to be identical to those of the corresponding symmetry-related residues in the first subunit.

the maximum of $\Delta\Delta G_{\text{self}}$ at the selectivity filter changes from ≈ 6 kcal/mol to ≈ 3 kcal/mol when we move from set A to set B. Although the treatment of set B is more consistent, we will use both profiles to assess the sensitivity of the calculations to the protein configurations used in the PDL/S calculations.

3.3. Effects of Ionizable Groups and Ion-Ion Interaction

The next step of our modeling involved an examination of the effect of charge–charge interactions on the penetration profile. First, we set all the ionized groups to their optimal ionization state at $\text{pH} = 7$. This was done by using the PDL/S-LRA to find the intrinsic $\text{p}K_a$ of each ionized residue and then using a self-consistent hybrid approach (see Sham et al.³⁵), with the charge–charge interaction term of eq. 7 for the interaction between the ionized residues, to determine their apparent $\text{p}K_a$ s. Our results are summarized in Table I. These results are probably reliable because of the use of the LRA averaging procedure in the PDL/S calculations. As a point of reference we can consider the Asp80 and Glu71 pair. At $\text{pH} = 7$ we find, in agreement with Luzhkov and Åqvist⁴⁶ and Ranatunga et al.,¹⁸ that Asp80 is ionized and Glu71 is protonated. However, we believe that the interaction between these two groups is somewhat overestimated in other studies (the calculated interaction is 10–13 kcal/mol in Luzhkov and Åqvist⁴⁶ and > 13 kcal/mol in Ranatunga et al.¹⁸). We obtained an interaction energy of ≈ 5 kcal/mol by direct PDL/S-LRA calculations that included the two groups explicitly and ≈ 5 kcal/mol by the use of eq. 7. Our extensive experience with experimentally based analysis of charge–charge interactions in proteins^{40,47} has indicated that these interactions are associated with a relatively large dielectric constant. Macroscopic models (e.g., Ranatunga et al.¹⁸) that use a small value for ϵ_p lead to

major overestimation and even FEP calculations lead to a significant overestimation of the charge–charge interactions due in part to the neglect of the effect of other ionized groups, which are not a part of the specific ion pair (see Sham et al.⁴⁷).

Interestingly, the ionization states of some groups depend significantly on the presence of the membrane (see Table I). Further, we also found dependence on the size of the membrane region (e.g., pK_{int} of Arg89 decreased by five units when the membrane width increased from 35 to 40 Å). This result is not likely to be an artifact of the simulation but a simple consequence of having a low dielectric region near ionizable residues. Of course, it is possible that water penetration into the membrane region will help stabilize the ionized form of the ionizable residues; however, the general trend of the effect of the membrane is most probably reproduced by the calculations.

The apparent pK_a s of the second column were used to determine the ionization state of the system. Because the channel is open at $\text{pH} \leq 4.6$ we “ionized” residues with more than 50% probability of being ionized at $\text{pH} = 4.6$. However, we also ionized Asp80 and kept Arg27 neutral because the apparent pK_a of these residues is 4.7 ± 0.5 . Now, we used eq. 1 with a single K^+ ion and produced the profiles shown in Figure 5 for two limits ($\epsilon' = 60$ and $\epsilon' = 30$) of the effective dielectric of eq. 7.

As seen from Figure 5, we obtained a substantial effect of the protein-ionizable groups. However, this effect is significantly smaller than that obtained by the macroscopic calculations of Ranatunga et al.¹⁸ because these calculations used a low ϵ_p without the LRA treatment. The problems in treating charge–charge interactions with low ϵ_p have been demonstrated in our previous works.^{38, 47}

In addition to the apparent pK_a s obtained by the above calculations (without any K^+ ions in the channel), we also evaluated the apparent pK_a s for the case where the channel contains a K^+ ion in the central cavity (see also Table I). Considering the corresponding ionization state and penetration profile might provide a more appropriate model for simulations of the current with more than one ion in the channel at any given time.

To validate some aspects of the above calculations, we examined the energetics of the KcsA channel in a more microscopic way by performing PLDL/S-LRA calculations that included explicitly the ionizable groups and the K^+ ions. This treatment obtained the effect of the ionizable groups through the use of eq. 5 rather than by the use of ϵ_{eff} . The calculations were done for selective sites, focusing on different “loading states” for the ions. These states were defined following Åqvist and Luzhkov¹⁶ in terms of the five sites in the channel, which are designated by a, b, c, d, and e in Figure 1. The five sites include four binding sites (which are separated by 3.4, 3.9, and 3.3 Å in the crystal structure) and a fifth position at the central water-filled cavity (see Åqvist and Luzhkov¹⁶ for details). The occupation of these sites is designated by 1 (occupied) and 0 (unoccupied) sites. Thus, (01000) corresponds to a single occupation of the second site. The results of the calculations,

with and without the protein-ionizable groups, are summarized in Table II. Now the effect of the ionized groups is larger than that obtained in Figure 4 with ϵ_{eff} . However, this effect is still smaller than the effect obtained in the macroscopic study of Shrivastava and Sansom.¹⁹ We also find that both of our semimacroscopic treatments give substantially less stabilization to the single ion configuration than those obtained by Luzhkov and Åqvist.⁴⁶ This difference reflects in part the use of a frozen channel in the single ion calculations of Luzhkov and Åqvist.⁴⁶ The procedure used in Luzhkov and Åqvist⁴⁶ was justified in view of the instability of the channel without any bound ion. However, it seems to us that the energetics associated with a large reorganization of the channel cannot be evaluated reliably by current microscopic calculations. Such calculations may overestimate the interaction of K^+ with the ionized groups without the inclusion of all the protein-ionized groups (and their mutual interactions) and/or without a complete reproduction of the effect of water penetration and other reorganization effects. These effects are implicitly included in our ϵ_p .

The results presented in Table II provide a useful way of assessing the validity of eq. 7 and the corresponding ϵ_{eff} . This can be done by comparing the semimacroscopic results to those obtained with ϵ_{eff} . For example, as seen from the tables, the free energy of placing K^+ in site c when site d is occupied by another K^+ ion is 8.8 kcal/mol higher than the corresponding energy when site d is empty. Using this information and eq. 6 gives (see also Sham et al.⁴⁷)

$$\begin{aligned} \Delta G[(00010) \rightarrow (00110)] - \Delta G[(00000) \rightarrow (00100)] \\ = 332/r_{cd}\epsilon(r_{cd}) = (11.4 - 2.6)\text{kcal/mol}, \quad (12) \end{aligned}$$

with $r_{cd} = 3.3$ Å we obtain $\epsilon(3.3) \approx 11.3$ as compared to the value of 17.8 obtained from eq. 7. The same analysis for the interaction between sites a and c gives $\epsilon(7) \approx 17$ for the unionized protein and $\epsilon(7) \approx 17$ for the ionized protein, as compared to the value of 32.1 obtained from eq. 7. Analysis of the interaction between different sites gives similar results, where the direct calculation gives a dielectric constant that is usually smaller than the value obtained from eq. 7. However, our experience from comparison of PDL/S calculations to the corresponding experimental information is that the calculated interactions overestimate the observed values. Thus, we believe that the use of eq. 7 captures the average trend even for interactions between neighboring K^+ ions. At any rate, we will also consider a lower limit for ϵ_{eff} using eq. 7 with $\epsilon' = 30$ [the corresponding single ion profile is presented in Fig. 5(b)]. We also attempted to account for the fact that ϵ_{eff} is large when the two interacting ions are in water and when a charged group on the surface of the protein interacts with another ionized group or with a K^+ ion. Thus, we used $\epsilon' = 80$ in eq. 7 for interaction between ions in water and for interaction between an ion and an ionized protein group located at less than 2 Å from the protein/water interface.

One interesting feature of the calculated profile is the relatively large barrier (≈ 10 kcal/mol) at the “gate” region ($-30 \text{ Å} < z < -14 \text{ Å}$). Although this calculated free energy

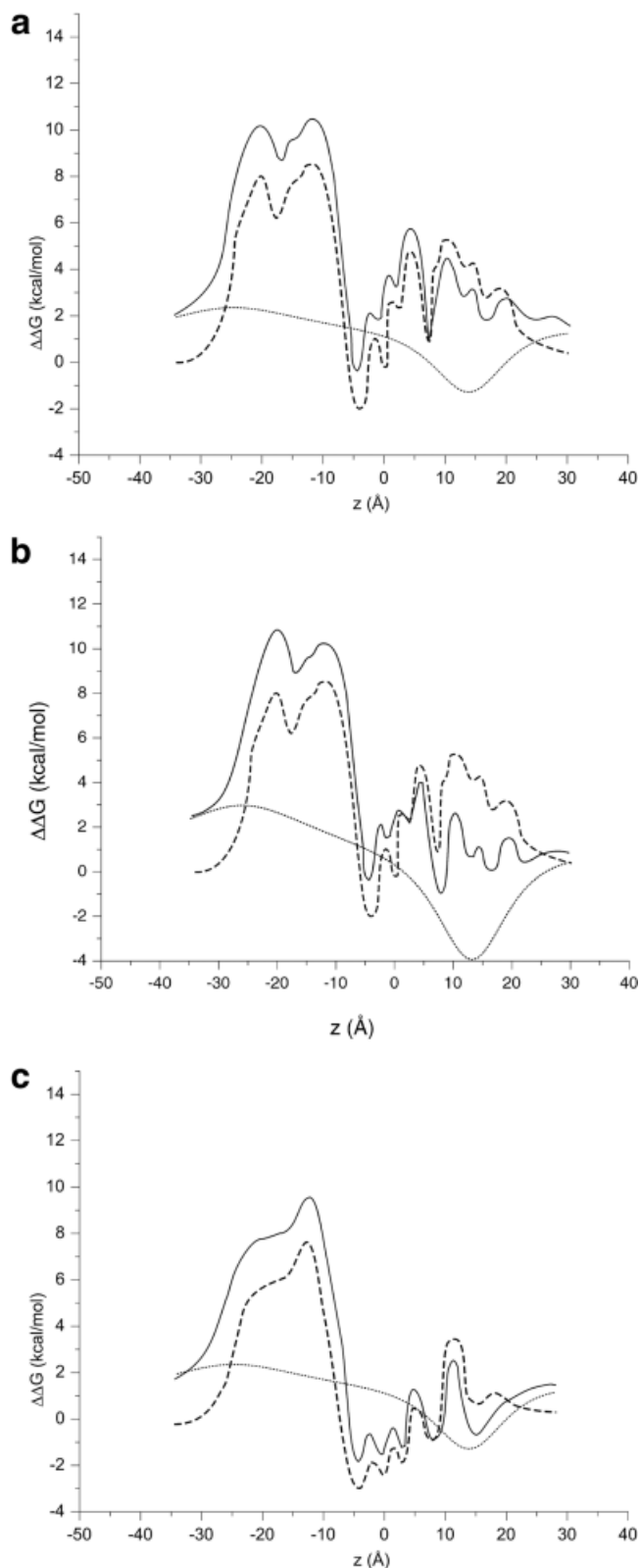


TABLE II. PDLD/S-LRA Energetics of Different Configurations of K^+ Ions in the KcsA Channel

Configurations ^a		$\Delta\Delta G$ (kcal/mol) ^b	
Initial	Final	Unionized protein	Ionized protein
00000	(1)0000	4.4 (4.0)	-0.1
00000	0(1)000	0.6 (-1.0)	-5.6
00000	00(1)00	2.6 (-2.0)	-3.7
00000	000(1)0	-0.2 (-2.8)	-2.6
00000	0000(1)	-2.2 (-3.1)	-6.7
00001	(1)0001	5.8	0.8
00001	0(1)001	0.3	-4.9
00001	00(1)01	3.1	-1.0
00001	000(1)1	3.9	4.7
01000	(1)1000	12.2	9.7
00100	(1)0100	9.6	2.8
00010	(1)0010	7.8	0.3
00100	0(1)100	9.2	4.5
00010	0(1)010	6.4	-1.1
00010	00(1)10	11.4	3.1
01001	(1)1001	14.2	10.5
00101	(1)0101	8.6	3.0
00011	(1)0011	7.5	4.4
00101	0(1)101	11.4	3.4
00011	0(1)011	6.0	-0.3
00011	00(1)11	13.0	7.0

^aThe ions that were included in region I are given in parentheses.

^bValues in brackets correspond to PDLD/S-LRA calculations with configurations generated using induced-dipoles forces.

barrier is much smaller than the barrier obtained by other approaches (e.g., Ranatunga et al.¹⁸ obtained a barrier of ≈ 120 kcal/mol from the interaction energies evaluated by short MD simulations), it is still too high to account for the observed current. That is, a barrier of ≈ 10 kcal/mol corresponds to a rate constant in the range of $\approx 4 \cdot 10^5 s^{-1}$ as estimated by transition state theory (e.g., Warshel⁴⁸). The effect of diffusion on the barrier and the transmission factor may reduce this value to less than $10^5 s^{-1}$. This rate constant is too small to account for the rate of ion flow through the KcsA channel, which is in the range of $10^7 s^{-1}$. Although we will explore this issue in a more quantitative way in the next sections, it seems to be consistent with the belief that the X-ray structure corresponds to a closed state of the channel.^{49–51} In view of this we performed the simulations while scaling down the barrier at the gate region (see Section 3.4).

3.4. Single-Ion Trajectories

As a first step of our ion current simulations we explored single-ion trajectories. This was done using eq. 9 with $\gamma_c =$

Fig. 5. Effect of the protein-ionizable groups on the single-ion penetration profile. The calculations correspond to the first and third terms of eq. 1. The figure depicts the $\Delta\Delta G_{\text{self}}$ (broken line) and the corresponding total penetration potential (solid line). The contribution of the interaction between the ionizable groups and the K^+ ion is given by a dotted line. The results obtained from set A, using the effective dielectric of eq. 7 with $\epsilon' = 60$ and $\epsilon' = 30$ are given in (a) and (b), respectively. The full penetration potential of set B, with $\epsilon' = 60$, is shown in (c).

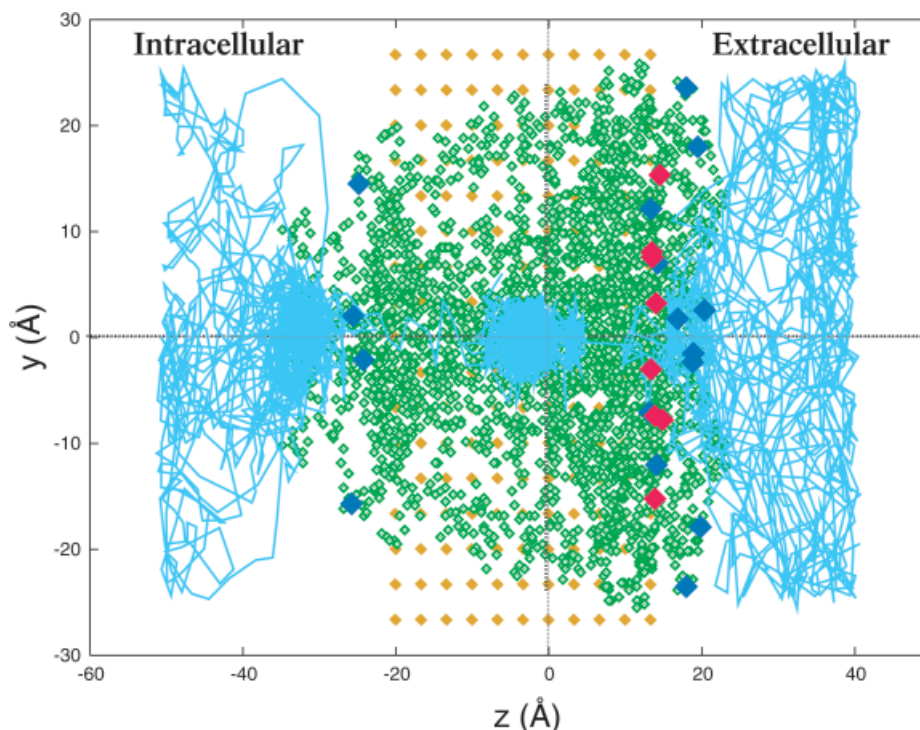


Fig. 6. Single-ion trajectory. The figure describes the result of a 100-ns BD simulation. The protein is shown in green and the ionized groups are shown in red (negative) and blue (positive), respectively.

$\gamma_w = 33 \text{ ps}^{-1}$. These simulations involved the free energy function of eq. 1 with the $\Delta\Delta G_{\text{self}}$ obtained without the induced-dipoles forces (set A). The simulations could not produce any productive trajectory during a microsecond simulation time. That is, trajectories that started from the intracellular side were unable to pass the barrier at the gate region, while trajectories that started from the extracellular region arrived at the central cavity but were again unable to pass the barrier at the gate region. This problem reflects the fact that the gate region is most probably in its closed form (see Section 3.3). In the absence of a structural model for the open state of the gate we decided to force the system to behave as if it has an open gate. There are several feasible ways to try to accomplish this but a quantitative attempt should involve more structural information. Thus, we simply reduced the barrier at the gate region to 2 kcal/mol, leaving the selectivity filter unchanged. The assumption that the structure (and thus the barrier) in the selectivity filter does not change in a major way between the open and closed states of the channel is consistent with mutation experiments. Admittedly our treatment of the gate region is an arbitrary one, but it is probably as reasonable as anything that can be done before we try to generate structural models of the open state. At any rate, after scaling the barrier in the gate region we were able to generate single-ion trajectories that passed the channel in a microsecond time scale. Other trajectories did not pass the channel even after 5 ms. Using the $\Delta\Delta G_{\text{self}}$ of set B (where $\Delta\Delta G^{\ddagger} \cong 3 \text{ kcal/mol}$) gave an average passage time of $\approx 100 \text{ ns}$. Similar results were obtained by taking the $\Delta\Delta G_{\text{self}}$ of set A and scaling it down by 0.5. A

typical single-ion trajectory, which was obtained with set B, is shown in Figure 6.

3.5. Simulating Ion Current in the KcsA Channel

After the preliminary study of Section 3.4 we moved to the more meaningful simulations of the overall ion current. Because our work focused on the demonstration of the method rather than on the reproduction of the actual current for different concentration gradients, we considered only one concentration gradient. That is, the system was set with 4 ions of K^+ and 4 ions of Cl^- in the extracellular side and 8 ions of K^+ and 8 ions of Cl^- in the intracellular side. This corresponds to concentrations of 200 and 400 mM in the extracellular and intracellular sides, respectively. These concentrations are larger than the typical experimental concentrations (see below), but provide a better statistics for the current calculations. The results of the simulations should be compared to the experimental finding⁵² of a K^+ current of 2 pA for a concentration ratio, $(C_{\text{in}}/C_{\text{out}})$, of 250 mM/125 mM. A rough extrapolation of this result to our simulation conditions can be obtained from the Nernst-Planck equation (e.g., Hille¹). At zero potential one finds (e.g., eq. 13-13 of Hille¹) that the current is proportional to $|C_{\text{in}} - C_{\text{out}}|$. This means that the “experimental” result at the simulation conditions should be around 4 pA.

The actual calculations for the K^+ current are summarized in Table III. These calculations examined the dependence of the simulated current on several key features as well as the performance of the method for the most reasonable set. This includes changing the friction between its limiting values, scaling down the ΔG_{self} profile of

TABLE III. Simulated Ion Current in the KcsA Channel[†]

γ_w, γ_c^a	$\Delta\Delta G_{\text{self}}^{\ddagger}$ (kcal/mol) ^b	ϵ'^c	I (pA)
33, 66	6.0	60	$\geq 0.01^d$
33, 66	5.0	60	0.06
33, 66	4.0	60	0.12
33, 66	3.0 (set B)	60	1.0
10, 10	4.0	60	0.8
10, 10	3.0 (set B)	60	5.0
33, 66	4.0	30	0.3
33, 66	2.0	60	1.0
33, 66	2.0	60	2.0

[†]Calculations were done with a concentration of 400 and 200 mM in the intracellular and extracellular regions, respectively.

^aThe friction coefficients for the water (w) and the channel (c) regions are given in ps^{-1} .

^b $\Delta\Delta G_{\text{self}}$ is the maximum of the $\Delta\Delta G_{\text{self}}$ profile in the region of the selectivity filter. The notation set B indicates that the calculations were done with the profile of set B. All other calculations were done with profiles obtained by either set A or by scaling down the profile of this set.

^cValue of the ϵ' for the effective dielectric function of eq. 7.

^dThis calculation requires a long simulation time and involves a poor statistics.

set A, using set B, and changing ϵ' from 60 to its lower limit of 30. As seen from table the current obtained with set A ($\Delta\Delta G_{\text{self}} = 6$ kcal/mol), $\gamma_c = 66 \text{ ps}^{-1}$, and $\epsilon' = 60$ underestimated the observed current by more than a factor of 100. More reasonable results were obtained both with the $\Delta\Delta G_{\text{self}}$ of set B and by scaling down the $\Delta\Delta G_{\text{self}}$ of set A. We consider these results, and in particular those obtained with set B (which is the more reasonable set), encouraging in view of the somewhat preliminary nature of the calculation. We find it useful to point out that other calculations, which were able to reproduce the observed current, succeeded to do so by an arbitrary selection of the protein dielectric constant or related parameters (see Section 4). To learn in a qualitative way about the nature of the ion flow we considered the simulation with set B and $\gamma_c = 66 \text{ ps}^{-1}$. The trajectories obtained from this simulation were used to evaluate the probability distribution for the K^+ ions. The resulting distribution, which is depicted in Figure 7, appears (as it should) to correspond to the underlined free energy profile, that is, the largest probability of finding the ions inside the channel corresponds to the central cavity. Similarly, the probability of finding the ions in the high-energy region of the selectivity filter is small.

Some interesting aspects of the trajectories involved in the ion flow are summarized in Figure 8. The figure considers a multi-ion trajectory, obtained with set B, and shows the time dependence of the coordinates of three K^+ ions during a penetration event. The figure depicts interesting information about the correlated motion of some of the ions. In this specific case the ion in the central cavity appears to move toward the selectivity filter while another ion moves from the selectivity filter to the extracellular direction. The motion of the three ions is also described in the upper part of the figure, which shows snapshots of the positions of the ions. It is not yet clear if this type of reactive trajectory is related to the concerted motion deduced from the insightful free energy

calculation of Åqvist and Luzhkov¹⁶ and supported by more recent considerations.^{32,53} It is still possible that the picture of a concerted motion is not as general as currently assumed. This issue cannot be resolved at present from MD simulations because they cannot generate the ion distribution that corresponds to the overall current flow. Assuming that the initial conditions for the MD simulations correspond to the observed occupation of the loading states might not be fully justified. A more conclusive analysis may be obtained by generating different ion configurations from our BD simulations and then conducting detailed MD studies of specific reactive trajectories. At any rate, a more detailed examination of the nature of the “reactive” trajectories is left for subsequent studies. However, some general conclusions can be already drawn from Table III. In particular, it appears that the magnitude of the calculated current is most sensitive to the activation barriers in the selectivity filter.

4. DISCUSSION

In this work we developed an approach for the simulation of ion current in realistic models of biologic ion channels. Our method combines a structure-based semi-macroscopic approach with BD simulations. The use of a semimacroscopic electrostatic model allowed us to represent the overall energetics in the channel in a relatively accurate way. This was done while taking into account, in a computationally affordable formulation, the self-energy of each ion and its interaction with all other charged groups (other ions and ionized residues). The use of BD simulations allowed us to overcome the serious limitation on the length of MD trajectories with all-atom potential surfaces. The effectiveness of our approach was demonstrated in a study of the ion current in the KcsA channel.

The idea of using BD for ion channel simulations is clearly not new (see Section 1) and not the central point of the present work. In our opinion what is new and significant is the generation of a reliable effective potential that reflects all the key features of the channel. To distinguish this potential from those used in related studies we refer to our model as a “realistic model.” Of course, “realistic” is a relative term and all-atom models are more realistic. However, such models cannot be used at present for current calculations. To clarify the advantages of our effective potential we will provide below a discussion of other treatments.

Attempts to combine BD simulations with PB calculations were reported for ion transport in a model of porin.^{54,55} However, porin provides a wide pore that yields a flat and simple penetration profile. In such cases the simulations are not drastically different than studies of ion mobility in water or in simple wide channels.^{54–56} Here one does not face any of the crucial challenges that appear in the KcsA and related narrow ion channels, where many models give unrealistic penetration barriers. In fact, all the treatments that gave unsatisfactory results in KcsA would give reasonable result in porin.

Although the use of PB continuum models provides a way for exploring some features of ion transport, their current combination with BD does not allow for sufficiently fast

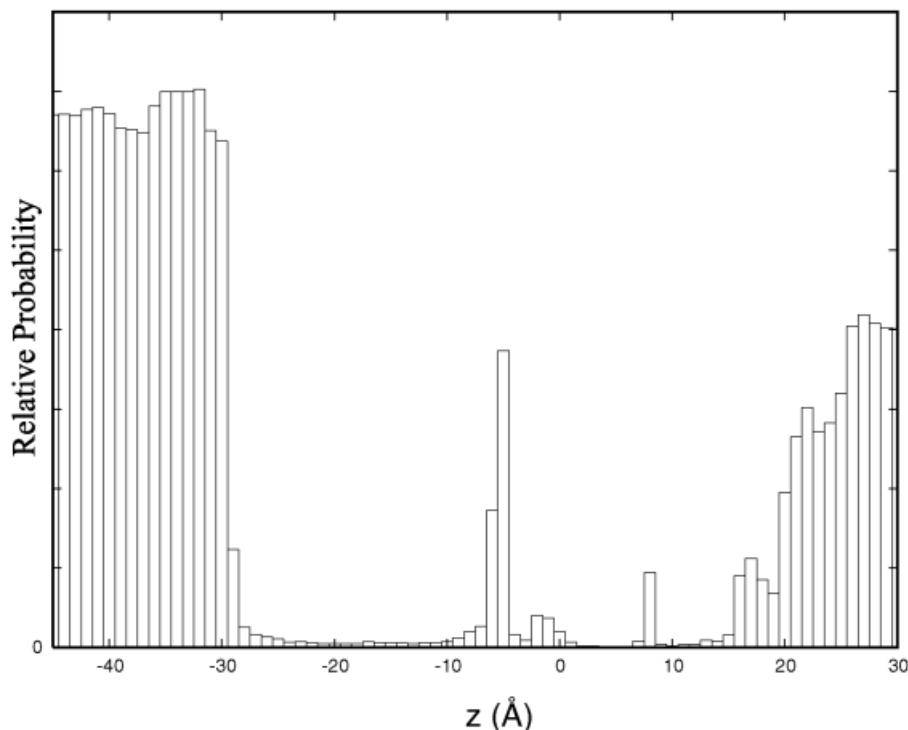


Fig. 7. Probability profile obtained from the multiion simulations described in the text.

calculations. The main problem is associated with the need to perform PB calculations for each configuration of the moving ions. This cannot be done with a single evaluation of the potential from the surrounding because this potential should reflect the reaction field from the ions (whose positions are constantly changing). The situation is expected to be particularly serious when several ions are in a close distance (in this case the change in the reaction field determines the effective repulsion between the ions). A related problem exists with respect to the dielectric constant, ϵ_p , used in PB calculations. The use of a small ϵ_p is a reasonable approximation for the self-energy but a poor one for the charge–charge interaction in protein interiors.³⁰

In general, it is easy to obtain a reasonable ion current by adjusting parameters in phenomenological models or by adjusting the dielectric constant in macroscopic models (e.g., Chung et al.²³). Such approaches can be instructive in teaching us about the general trend, but they do not necessarily reflect correctly the different contributions of the system. For example, several works have focused on the variation of the “dielectric constant” of the water molecules, ϵ_w , inside the channel (e.g., Chung et al.²³) while using a low dielectric for the protein. Such a treatment leads to incorrect electrostatic interactions in cases of narrow channels, where the effect of changing ϵ_w between, say, 80–30 is trivial relative to the poor approximation of using $\epsilon_p = 2$. These problems are not obvious unless one calculates the effect of the protein-ionized groups, which would be drastically overestimated. Here, the ability to obtain a realistic description of the different electrostatic contributions is essential for reliable prediction of the effect of mutation on the ion current.

A more subtle problem occurs in a recent work (Mashl et al.⁵⁷) that appeared after the submission of this article. This work presented an elegant treatment of ion current in KcsA using a 1-D LD simulation, based on a free energy profile obtained by a PB treatment with $\epsilon_p = 20$, and with ion–ion dielectric constant of 20. As was shown repeatedly in our works,³⁰ the use of $\epsilon_p \geq 20$ gives reasonable results for charge–charge interactions but poor results for charge–dipole interactions (where $\epsilon_p \leq 6$ gives much more realistic results). The use of $\epsilon_p = 20$ leads to a disappearance of the barrier in the gate region, even in the closed form of the gate, and to a more or less featureless potential in the selectivity filter. The loss of the strong dipole–charge interaction in the selectivity filter may lead to major difficulties in modeling and predicting ion selectivity.

The above problems are reduced by our semimacroscopic treatments. First, the use of the LRA treatment provides a relatively reliable treatment of the self-energy term, while taking into account the protein reorganization at each site. This allows one to use a less arbitrary ϵ_p (see Schutz and Warshel³⁰). Second, the use of our implicit $\epsilon_{\text{eff}}(r)$ for charge–charge interactions allows for an effective and reliable evaluation of the energy of the interacting charges in different configurations during the trajectory of the multiion system. The use of eqs. 4, 5, and 6 accounts for the overall response of the environment to the change in the ions’ position. This includes the protein reorganization, water penetration, and movements of surrounding ionized groups. Some of these effects are hard to capture reliably by more macroscopic treatments.

We would like to emphasize at this point that the changes of ϵ_{eff} between its lowest and highest limit are

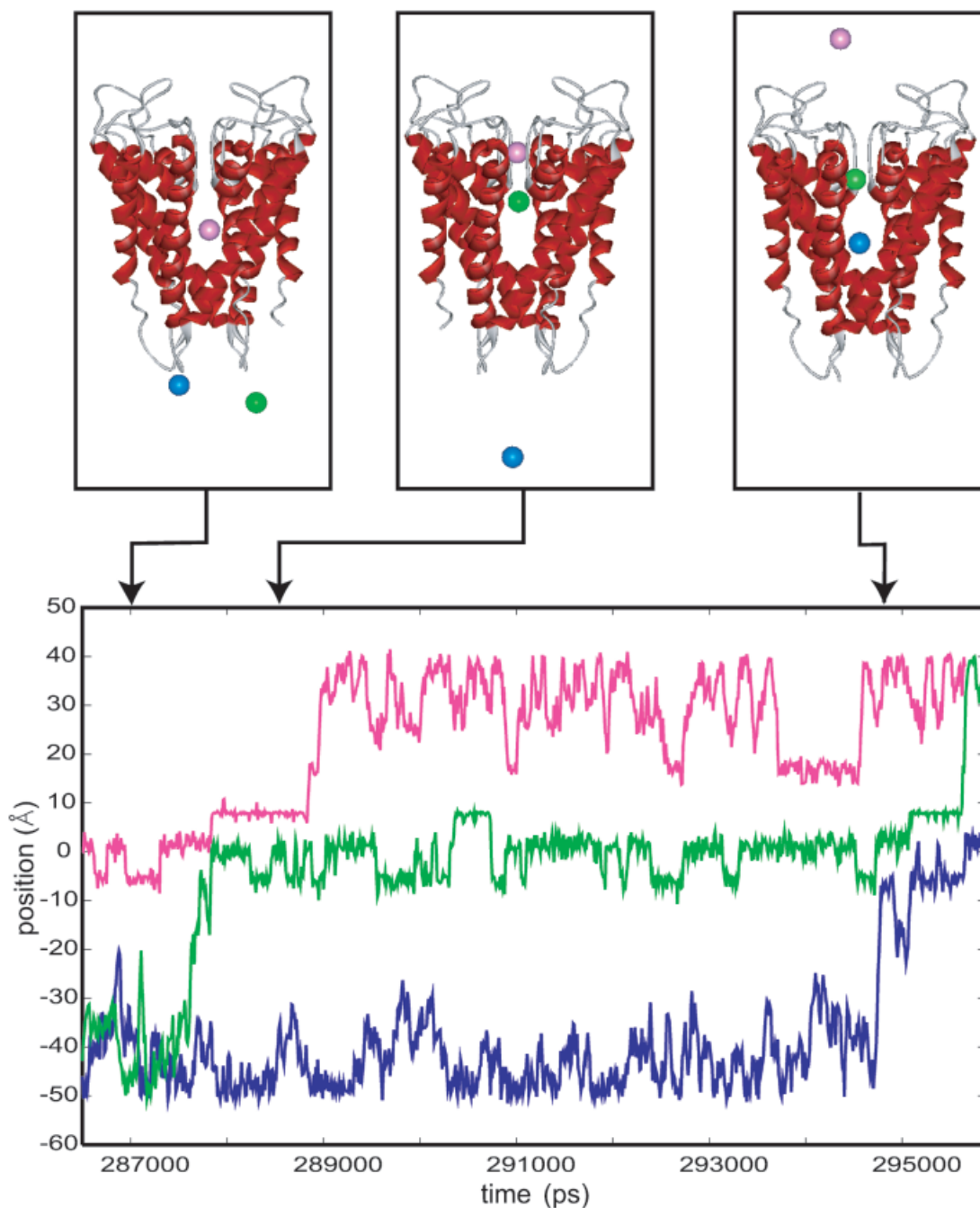


Fig. 8. Section of a multiion trajectory obtained with set B and concentrations of 400 and 200 mM in the intracellular and extracellular sides, respectively. The figure shows the time-dependent positions along the z axis of three K^+ ions during a penetration event. The upper figure shows snapshots of the channel and the three K^+ ions.

much less arbitrary than the selection of parameters in the above-mentioned macroscopic models. In both limits of our ϵ_{eff} we have a *large* screening of charge–charge interactions and the differences in the calculated energies are not large. It appears to us that the error limit of our approach, which we estimate to be in the range of ≈ 2 kcal/mol (with set B), is a significant advance as much as general treatment of ion channels is concerned. The issue is not a reproduction of a small barrier for a biologically optimized

channel, but the ability to obtain a reasonable prediction of the barrier height when the barrier is significant (e.g., the barrier for Na^+ and the effect of closed gate).

At the risk of repetition and in response to a concern of a referee of this work, we would like to further clarify and summarize why we consider our work to be a significant advance over previously published macroscopic models. The error range of our approach (which we estimate to be one order of magnitude in the predicted current) might

seem large in view of the success of macroscopic models that use a large ϵ_p to produce a reasonable current. However, as stated above, optimal open channels have low barriers of less than 3 kcal/mol and such low barriers are trivially reproduced by models of large ϵ_p . The problem is that such models will lead to almost no barrier for closed channels or for channels not optimized by evolution. If one deals with a closed channel with a barrier of 8 kcal/mol, he will obtain from a model with $\epsilon_p = 20$ a barrier of about 2 kcal/mol and an error of more than five orders of magnitude in the predicted current. A similar problem will occur in studies of ion selectivity (see above). On the other hand, models that use $\epsilon_p \leq 4$ will drastically overestimate the effects of ionized residues and ion-ion interactions.

Before concluding the discussion of the energetics obtained by our model it might be useful to comment on the option of using more microscopic models for the evaluation of the self-energy. Here it is clear that the optimal approach should eventually involve all-atom free energy simulations. However, it is not clear that such an approach can give at this stage more reliable results than those obtained by the present approach. That is, as discussed in Section 3.3, the careful FEP calculations of Luzhkov and Åqvist⁴⁶ probably overestimated the interactions between the protein-ionized groups and the K^+ ions. In this respect one may assume that the PMF calculations of Berneche and Roux³² represent more stable results than those obtained by FEP calculations. Unfortunately, the PMF calculations do not tell us much about the absolute binding energy of the ions (the energy of the ions in the protein relative to their energy in water). The finding that the PMF gives a small barrier for ion motion in the selectivity filter does not mean that it will give a small barrier for moving these ions from water to the selectivity filter. In fact, if it was possible to use PMF calculations to evaluate the absolute "binding" energy of the ions we would have probably obtained the same (or larger) effects of the ionized residues as those obtained by FEP calculations (depending, of course, on the overall treatment of long-range effects). At any rate, it is impossible to reach a clear conclusion about the mechanism of ion transport without evaluating the energy of moving these ions from water to their site.

We would like to emphasize that the above discussion is not presented as a criticism of different treatments, which certainly provided a useful insight, but is an attempt to emphasize the specific advantages of the current model. Obviously, our approach is not perfect and can be improved. For example, it would be useful to try to evaluate $\Delta\Delta G_{\text{self}}$ values at the minima of this profile by the PDL/D/S method or by a FEP approach, and then evaluate the PMF between the minima by an umbrella sampling or a related approach. In particular, it would be important to reproduce experiments about the relative binding energies of different ions in different sites^{14,53} to validate and refine the optimal method.

Another aspect that should be improved is the selection of the proper γ_c and r^* . These two parameters are somewhat correlated and have a nonnegligible effect on the calculated current. In view of the problems mentioned in Section 2.2, it would be useful to refine these parameters

by comparing the BD calculations to the corresponding all-atom MD simulations of the ion motion at the filter region. In doing so it might be also useful to consider the time dependence of the dielectric constant. That is, our study used ϵ_p and ϵ_{eff} that correspond to a fully relaxed environment (or to the long-time component of the dielectric "constant"). However, the electrostatic response of the environment is a time-dependent process and in cases of fast charge transfer reactions we should consider the fact that the environment may not be fully relaxed.²⁷ This effect can be simulated by assigning time dependency to ϵ_{eff} .²⁸ The characteristic time dependence can be estimated from macroscopic simulations.

The ability to simulate ion current is instructive and potentially important. Yet, the overall penetration time seems to be determined mainly by the energetics of the system. That is, once the nature of the rate-determining state is elucidated it is possible to evaluate the activation barrier along the corresponding reaction path and apply transition-state theory (TST) with a correction that reflects the corresponding transition factor (e.g., see Villà and Warshel⁵⁸). In fact, TST has been used effectively in analyzing ion channels (e.g., Åqvist and Luzhkov¹⁶ and Miller⁵⁹). Nevertheless, in cases that involve several ions, the use of BD may be crucial for finding out the mechanism of penetration through the bottleneck of the system.

Our study presented a somewhat preliminary exploration of the KcsA channel and produced a reasonable current without a major adjustment of the parameters used (see discussion above). However, a more critical test would require calculations of the effect of mutations and changes of the cations on the calculated current. Such calculations will be reported in the future. At the present stage we believe that at least one of our conclusions is likely to hold in more systematic studies. That is, our finding that the barrier at the gate region corresponds to a closed state of the channel is most probably valid. This conclusion is consistent with the current view that the structure of the KcsA channel corresponds to the situation where the gate is closed.^{49–51} It would be interesting to try to use simulation and/or experimental information to generate the open state of the channel.

ACKNOWLEDGMENTS

This work was supported by the National Institutes of Health, Grant GM40283. J.V. acknowledges EMBO fellowship ALTF 509-1998. We thank USC ISD for computer time.

REFERENCES

1. Hille B. Ionic channels of excitable membranes, 2nd ed. Sunderland, MA: Sinauer Associates; 1992.
2. Lauger P. Ion transport through pores: a rate-theory analysis. *Biochim Biophys Acta* 1973;311:423–441.
3. Eisenman G, Horn R. Ionic selectivity revisited: the role of kinetic and equilibrium processes in ion permeation through channels. *J Membr Biol* 1983;50:1025–1034.
4. Latorre R, Miller C. Conduction and selectivity in potassium channels. *J Membr Biol* 1983;71:11–30.
5. Jordan PC. Microscopic approaches to ion transport through

- transmembrane channels. The model system gramicidin. *J Phys Chem* 1987;91:6582–6591.
6. Jakobsson E, Chiu S-W. Stochastic theory of ion movement in channels with single-ion occupancy. *Biophys J* 1987;52:33–45.
 7. Jordan PC. Ion–water and ion–polypeptide correlations in a gramicidin-like channel: a molecular dynamics study. *Biophys J* 1990;58:1133–1156.
 8. Åqvist J, Warshel A. Energetics of ion permeation through membrane channels. Solvation of Na^+ by gramicidin A. *Biophys J* 1989;56:171–182.
 9. Roux B, Karplus M. Ion transport in the gramicidin channel: Free energy of the solvated right-handed dimer in a model membrane. *J Am Chem. Soc* 1993;115:3250–3260.
 10. Elber R, Chen DP, Rojewski D, Eisenberg R. Sodium in gramicidin: an example of a permion. *Biophys J* 1995;68:906–924.
 11. Parsegian A. Ion–membrane interactions as structural forces. *Ann NY Acad Sci* 1975;264:161–179.
 12. Warshel A, Parson WW. Dynamics of biochemical and biophysical reactions: insight from computer simulations. *Q Rev Biophys* 2001; 34:563–679.
 13. Doyle DA, Cabral JM, Pfuetzner RA, Kuo AL, Gulbis JM, Cohen SL, Chait BT, MacKinnon R. The structure of the potassium channel: Molecular basis of K^+ conduction and selectivity. *Science* 1998;280:69–77.
 14. LeMasurier M, Heginbotham L, Miller C. J KcsA: It's a potassium channel. *Gen Physiol* 2001;118:303–313.
 15. Fedida D, Hesketh JC. Gating of voltage-dependent potassium channels. *Prog Biophys Mol Biol* 2001;75:165–199.
 16. Åqvist J, Luzhkov V. Ion permeation mechanism of the potassium channel. *Nature* 2000;404:881–884.
 17. Luzhkov V, Åqvist J. K^+/Na^+ selectivity of the KcsA potassium channel from microscopic free energy perturbation calculations. *Biochim Biophys Acta* 2001;1548:194–202.
 18. Ranatunga KM, Shrivastava IH, Smith GR, Sansom MSP. Side-chain ionization states in a potassium channel. *Biophys J* 2001;80: 1210–1219.
 19. Shrivastava IH, Sansom MSP. Simulations of ion permeation through a potassium channel: Molecular dynamics of KcsA in a phospholipid bilayer. *Biophys J* 2000;78:557–570.
 20. Allen TW, Kuyucak S, Chung SH. Molecular dynamics study of the KcsA potassium channel. *Biophys J* 1999;77:2502–2516.
 21. Levitt DG. Interpretation of biologic ion channel flux data: reaction-rate versus continuum theory. *Annu Rev Biophys Chem* 1986;15: 29–57.
 22. Lee FS, Warshel A. A local reaction field method for fast evaluation of long-range electrostatic interactions in molecular simulations. *J Chem Phys* 1992;97:3100–3107.
 23. Chung SH, Allen TW, Hoyle M, Kuyucak S. Permeation of ions across the potassium channel: Brownian dynamics studies. *Biophys J* 1999;77:2517–2533.
 24. Eisenberg RS. From structure to function in open ionic channels. *J Membr Biol* 1999;171:1–24.
 25. Kurnikova MG, Coalson RD, Graf P, Nitzan A. A lattice relaxation algorithm for three-dimensional Poisson–Nernst–Planck theory with application to ion transport through the gramicidin a channel. *Biophys J* 1999;76:642–656.
 26. Åqvist J, Luecke H, Quirocho FA, Warshel A. Dipoles localized at helix termini of proteins stabilize charges. *Proc Natl Acad Sci USA* 1991;88:2026–2030.
 27. Warshel A. Conversion of light energy to electrostatic energy in the proton pump of *Halobacterium halobium*. *Photochem Photobiol* 1979;30:285–290.
 28. Warshel A. Correlation between structure and efficiency of light-induced proton pumps. In: Packer L, editor. *Methods in enzymology*. London: Academic Press; 1986. pp. 578–587.
 29. Sham Y, Muegge I, Warshel A. Simulating proton translocations in proteins: Probing proton transfer pathways in the *Rhodospirillum rubrum* reaction center. *Proteins* 1999;36:484–500.
 30. Schutz CN, Warshel A. What are the dielectric “constants” of proteins and how to validate electrostatic models. *Proteins* 2001; 44:400–417.
 31. Hu JS, Goldman S, Gray CG, Guy HR. Calculation of the conductance and selectivity of an ion-selective potassium channel (IRK1) from simulation of atomic scale models. *Molec Phys* 1999;98:535–547.
 32. Berneche S, Roux B. Energetics of ion conduction through the K^+ channel. *Nature* 2001;414:73–77.
 33. Warshel A, Sussman F, King G. Free energy of charges in solvated proteins: Microscopic calculations using a reversible charging process. *Biochemistry* 1986;25:8368–8372.
 34. Lee FS, Chu ZT, Bolger MB, Warshel A. Calculations of antibody–antigen interactions: Microscopic and semi-microscopic evaluation of the free energies of binding of phosphorylcholine analogs to McPC603. *Protein Eng* 1992;5:215–228.
 35. Sham YY, Chu ZT, Warshel A. Consistent calculations of pK_a 's of ionizable residues in proteins: Semi-microscopic and macroscopic approaches. *J Phys Chem B* 1997;101:4458–4472.
 36. King G, Warshel A. A surface constrained all-atom solvent model for effective simulations of polar solutions. *J Chem Phys* 1989;91(6): 3647–3661.
 37. Lee FS, Chu ZT, Warshel A. Microscopic and semimicroscopic calculations of electrostatic energies in proteins by the POLARIS and ENZYME programs. *J Comput Chem* 1993;14:161–185.
 38. Warshel A, Papazyan A. Electrostatic effects in macromolecules: Fundamental concepts and practical modeling. *Curr Opin Struct Biol* 1998;8:211–217.
 39. Hassan SA, Guarnieri F, Mehler EL. A general treatment of solvent effects based on screened Coulomb potentials. *J Phys Chem B* 2000;104:6478–6489.
 40. Alden RG, Parson WW, Chu ZT, Warshel A. Calculations of electrostatic energies in photosynthetic reaction centers. *J Am Chem. Soc* 1995;117:12284–12298.
 41. Warshel A, Russell ST, Churg AK. Macroscopic models for studies of electrostatic interactions in proteins: Limitations and applicability. *Proc Natl Acad Sci USA* 1984;81:4785.
 42. McQuarrie DA. *Statistical mechanics*. New York: Harper and Row; 1976.
 43. Kubo R. The fluctuation-dissipation theorem. *Rep Progr Phys* 1966;29:255–284.
 44. Corry B, Kuyucak S, Chung SH. Tests of continuum of models of ion channels. II. Poisson–Nernst–Planck theory versus Brownian dynamics. *Biophys J* 2000;78:2364–2381.
 45. Warshel A, Levitt M. Theoretical studies of enzymatic reactions: Dielectric, electrostatic and steric stabilization of the carbonium ion in the reaction of lysozyme. *J Mol Biol* 1976;103:227–249.
 46. Luzhkov VB, Åqvist J. A computational study of ion binding and protonation states in the KcsA potassium channel. *Biochim Biophys Acta* 2000;1481:360–370.
 47. Sham YY, Muegge I, Warshel A. The effect of protein relaxation on charge–charge interactions and dielectric constants of proteins. *Biophys J* 1998;74:1744–1753.
 48. Warshel A. *Computer modeling of chemical reactions in enzymes and solutions*. New York: John Wiley & Sons; 1991.
 49. Minor DL Jr. Potassium channels: Life in the post-structural world. *Curr Opin Struct Biol* 2001;11:408–411.
 50. Heginbotham L, LeMasurier M, Kolmakova-Partensky L, Miller C. Single *Streptomyces lividans* K^+ channel: functional asymmetries and sidedness of proton activation. *J Gen Physiol* 1999;114:551–559.
 51. Prozo E, Cortes DM, Cuellar LG. Structural rearrangements, underlying K^+ channel activation gating. *Science* 1999;285:73–78.
 52. Miller C. Personal communication. 2001.
 53. Morais-Cabral J, Zhou Y, MacKinnon R. Energetic optimization of ion conduction rate by the K^+ selectivity filter. *Nature* 2001;414:37.
 54. Schirmer T, Phale PS. Brownian dynamics simulation of ion flow through porin channels. *J Mol Biol* 1999;294(5):1159–67.
 55. Im W, Seefeld S, Roux B. A grand canonical Monte Carlo–Brownian dynamics algorithm for simulating ion channels. *Biophys J* 2000;79:788–801.
 56. Jordan PC, Bacquet RJ, McCammon AJ, Tran P. How electrolyte shielding influences the electrical potential in transmembrane ion channels. *Biophys J* 1989;55:1041–1052.
 57. Mashl RJ, Tang Y, Schnitzer J, Jacobsson E. Hierarchical approach to predicting permeation in ion channels. *Biophys J* 2001;81:2473–2483.
 58. Villà J, Warshel A. Energetics and dynamics of enzymatic reactions. *J Phys Chem* 2001;7887–7907.
 59. Miller C. Ionic hopping defended. *J Gen Physiol* 1999;113:783–787.